ISA Transactions xxx (xxxx) xxx

Contents lists available at ScienceDirect

ISA Transactions

journal homepage: www.elsevier.com/locate/isatrans

Research article

Time-delay control scheme with adaptive fixed-time convergent super-twisting fractional-order nonsingular terminal sliding mode for piezoelectric displacement amplifier

Zhicheng Song, Linkang Wang, Jie Ling, Lingyu Wang, Jinjun Duan, Yaoyao Wang *, Bai Chen *

College of Mechanical and Electrical Engineering, Nanjing University of Aeronautics and Astronautics, Nanjing, China

ARTICLE INFO

Keywords:
Piezoelectric displacement amplifiers
Time-delay estimation
Fractional-order nonsingular terminal sliding mode
Adaptive fixed-time convergent super-twisting algorithm

ABSTRACT

Piezoelectric displacement amplifiers (PDAs) have been widely used in precision positioning fields. However, the inherent hysteresis and creep nonlinear effect of piezoelectric actuators (PEAs) and time-varying lumped disturbances bring extreme challenges to the precise motion control of PDAs. Although various control schemes based on PEAs have been developed and have shown significant results. However, due to the high sensitivity of precision positioning to environmental variations, the development and identification of accurate models and the control timeliness often become obstacles in engineering. To realize precise motion control of PDAs under complex lumped disturbances, a new time-delay control scheme (AFSTA-FONTSM) using an adaptive fixed-time convergent super-twisting algorithm (AFSTA) and a fractional-order nonsingular terminal sliding mode (FONTSM) is proposed. Specifically, the time-delay information obtained by time-delay estimation technology is used to estimate the lumped dynamic characteristic of the system, thus establishing a simple control framework without a system dynamic model. FONSTM is constructed as a sliding mode manifold, and satisfactory error dynamic characteristic is obtained. A new AFSTA is designed as the reaching law in the sliding mode phase. AFSTA has fixed-time convergence when the upper bound of lumped disturbances exists, which ensures the control timeliness. Benefiting from the newly designed adaptive algorithm, the upper bound value of lumped disturbances is no longer needed to determine the control gains, which effectively prevents overestimation of the control gains. Correspondingly, the convergence time of AFSTA is estimated, and the stability of the closed-loop system is analyzed by the Lyapunov theory. Three existing time-delay control schemes, namely MSTA-FONTSM, AMSTA-FONTSM, and ASTA-FONTSM are selected, and four scenes are designed for comparative experiments. The experimental results show that MSTA-FONTSM has the worst control performance among the four control schemes. For the step, and continuous cosine trajectories with periods of $T = 1$ s and $T = 2$ s, the root-mean-square error of the proposed AFSTA-FONTSM is reduced by 56.86%, 54.03%, and 50.24% compared with MSTA-FONTSM. For disturbance experiments under different loads, the control performance of the proposed AFSTA-FONTSM is still superior to the other three control schemes without load.

1. Introduction

Piezoelectric actuators (PEAs) have attracted much attention for their unique performance. They are becoming more fascinating for the precise positioning field due to their high resolution, high stiffness, high electromechanical coupling efficiency, and fast response, such as micro/nano stage [1,2], atomic force microscopy [3], vibration isolation platform [4], and so on. However, the motion range of PEAs is limited, and the piezoelectric displacement amplifiers (PDAs) are usually designed to increase the motion range of PEAs in practical engineering. One of the most typical applications is to replace the staff with a PDA to automatically complete the cell micromanipulation tasks, including puncture, injection, nuclear transplantation, and so on. In [5–7], the researchers designed different PDAs and controlled them to complete the cell puncture task. The diameter of a typical single cell is usually 10 to 500 μm [8]. Therefore, precise control is crucial for PDAs. However, it is challenging work to design a high-performance controller for PDAs used in the micromanipulation tasks. The main obstacles include the following three aspects: (1). PEAs exhibit inherent hysteresis and creep nonlinear effect, and time-varying lumped disturbances, which makes it

* Corresponding authors.
E-mail addresses: yywang_cmee@nuaa.edu.cn (Y. Wang), chenbye@126.com (B. Chen).

https://doi.org/10.1016/j.isatra.2023.12.017
Received 21 July 2023; Received in revised form 4 November 2023; Accepted 8 December 2023
Available online 13 December 2023

very difficult to establish an accurate system model [9]; (2). Due to (1), the performance of PEAs is limited, and the positioning accuracy will be seriously deteriorated, thus affecting control accuracy [10]; (3). Micromanipulation tasks are extremely sensitive to lumped disturbances, and some parameters of the whole system often change unexpectedly [11]. The controller should have the rapid convergent ability in the face of disturbances to ensure control timeliness.

To overcome these obstacles, many researchers have made efforts and several control schemes have been proposed for piezoelectric-driven mechanical systems, such as feedforward control [12,13], sliding mode control (SMC) [11,14], model predictive control [15], iterative learning control [1,16], and so on. As one of the most effective methods to deal with lumped disturbances, SMC and its variants have also been widely used in many fields. Their core content is to force the system state variables to reach the preplanned sliding mode manifold and to limit and remain on the sliding mode manifold as much as possible to ensure robustness. To further improve the local convergence characteristic of SMC, researchers have developed terminal sliding mode (TSM) [17], nonsingular TSM (NTSM) [18], and fractional-order NTSM (FONTSM) [5] respectively, and achieved satisfactory results. The above methods usually use switching elements to ensure that the system state variables reach the sliding mode manifold. Because the upper bound value of lumped disturbances is difficult to acquire in engineering, the large control gain is often applied to switching elements, which will lead to the well-known chattering phenomenon [19]. Researchers have proposed many methods to reduce chattering, such as upper bound layer [20], reaching law [5], adaptive law [21], high-order SMC (HOSMC) [22,23], and so on. Compared with other methods, HOSMC is more popular because of its good comprehensive performance.

As one of the most powerful second-order continuous HOSMC algorithms, the super-twisting algorithm (STA) has become a research hotspot in many fields, such as power networks [24], electromagnetic direct-drive pump [25], magnetic levitation systems [26], and so on. It hides the switching elements behind an integrator [27], which can significantly reduce chattering without losing robustness [26]. However, the dominant term of STA is square root convergence, which will lead to a slow system response [28]. To improve the convergence speed of STA, researchers have proposed several modified STA (MSTA). The most classic modified algorithm is to add linear feedback terms to STA [29,30], and the convergence speed is improved, but it also leads to undesired overshoot. A new MSTA with double closed-loop feedback is proposed from [31]. This MSTA adds a proportional and a damping factor to the differential and the integral term of the sliding mode variable, which improves the convergence speed and reduces overshoot. It is worth noting that the above STA and MSTA have been proven to be finite-time convergence. The convergence time is related to the initial value. For instance, micromanipulation tasks are extremely precise, and any disturbances may affect the accuracy of the operation. When the system suffers from large disturbances, it may significantly deviate from the desired trajectory, resulting in large initial tracking errors. For a larger initial value, the convergence time will be longer, which leads to the control timeliness not being guaranteed. Therefore, it is a problem worthy of attention to design a fixed-time convergent STA (FSTA) and apply it to micromanipulation tasks.

A FSTA presented in [32] contains too many interrelated control items, which makes the system more complicated. Basin et al. [33–35] have made a series of profound studies on the FSTA and estimated the convergence time. Although the above research has achieved gratifying results, they still need identification methods to obtain the system dynamics model, which may not be suitable for micromanipulation tasks under complex lumped disturbances.

The time-delay estimation (TDE) technology is an intuitive, efficient, and powerful tool to settle the above problems. The system dynamics can be effectively obtained only by using the time-delay information of the system state, and a simple framework is realized. Because of the above advantages, TDE technology has been broadly used in many fields, such as robot manipulator [36], exoskeleton [37], and so on. Meanwhile, the time-delay errors caused by TDE usually require a robust control strategy to further improve the control accuracy. Recently, a control scheme combining MSTA and TDE has been developed for the cable-driven manipulator [38]. In this scheme, the robust control strategy adopts FONTSM with better performance and achieves satisfactory results. However, the constant control parameters need to be calculated by the upper bound value of lumped disturbances [39], which is difficult to obtain in engineering. When the disturbances change obviously, using fixed gains may lead to poor control performance.

Inspired by the above essential issues, we propose a new time-delay control scheme with an adaptive FSTA (AFSTA) and a FONTSM (AFSTA-FONTSM). Firstly, the control framework without a system dynamic model is established using TDE to estimate the lumped dynamic characteristic. Next, based on the TDE control framework, the control scheme is developed with FONTSM and AFSTA as sliding manifold and reaching law, respectively, and a new adaptive algorithm is designed. Then, the convergence time of AFSTA is estimated in detail, and the stability of the closed-loop system is analyzed by the Lyapunov theory. Finally, the reliability and superiority of the proposed control scheme are verified by comparative experiments in different scenes.

To be specific, the main contributions of this paper are as follows:

1) to propose a new time-delay control scheme with AFSTA-FONTSM. TDE technology is applied to establish a simple control framework without a system dynamics model. FONTSM is used as the sliding mode manifold to obtain a more satisfactory error dynamic characteristic. A new AFSTA is proposed as the reaching law. Being different from the existing finite-time convergent MSTA [38], AMSTA [40], and ASTA [41], when the disturbances are bounded, AFSTA ensures control timeliness with fixed-time convergence. Therefore, it has a faster convergence speed in the sliding mode phase.
2) to propose a new adaptive algorithm. The adaptive algorithm can generate appropriate control gains. Its advantage is that it no longer requires the upper bound value of the lumped disturbances to determine the control gains, which effectively prevents the overestimation of the control gains.
3) to estimate the convergence time of AFSTA and give the stability proof of the closed-loop system using the Lyapunov theory.
4) to verify the reliability and superiority of the proposed AFSTA-FONTSM compared with the existing control schemes by comparative experiments in four scenes.

The rest of this paper is organized as follows: In Section 2, the new control scheme and adaptive algorithm are designed and discussed. Comparative simulations are performed in Section 3. Comparative experiments are carried out in Section 4. A conclusion is presented in Section 5. The nomenclature list, detailed convergence time estimation, and stability proof are given in the Appendix.

2. Control scheme

2.1. System dynamics model

Fig. 1 shows a PDA device made of aluminum alloy 7075, which is machined by electric discharge machining. It is composed of leaf flexure hinges and is driven by a PEA. The system can be equivalent to a second-order dynamic model with a hysteresis effect, which can be described as [5]:

$$m\ddot{x} + c\dot{x} + kx = T_{em}(u - h) - f_p \tag{1}$$

where m,c, and k represent mass, damping coefficient, and stiffness coefficient; $\ddot{x}$,$\dot{x}$, and$x$are acceleration, velocity, and displacement; $T_{em}$is the conversion coefficient; u is the input voltage; h is the hysteresis term; f_p

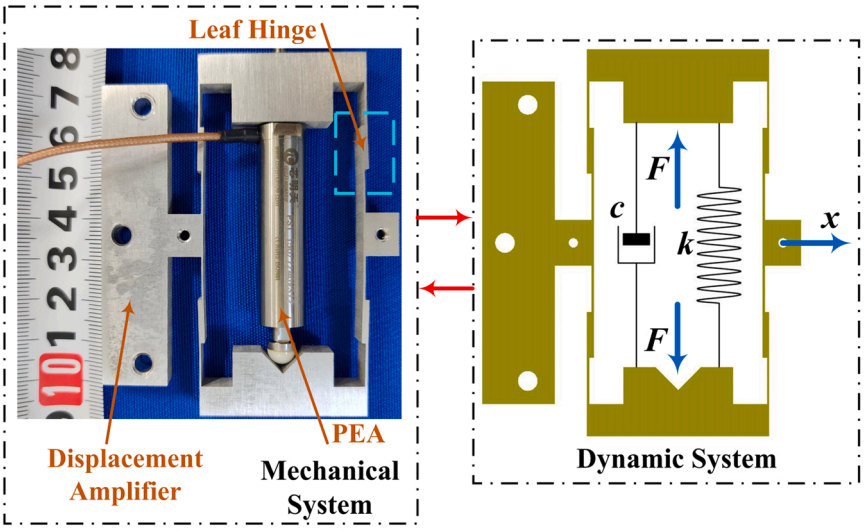

Fig. 1. Dynamic system of PDA.

are other unmodeled disturbances.

According to Eq. (1), the control input can be expressed as:

$$u = T_{em}^{-1}\left(m\ddot{x} + c\dot{x} + kx + f_p\right) + h \tag{2}$$

Because it is difficult to obtain T_{em} in practical engineering, we introduce a nominal value $\widehat{T}_{em}$ and Eq. (2) can be rewritten as:

$$u = \widehat{T}_{em}^{-1} m\ddot{x} + H \tag{3}$$

where:

$$H = T_{em}^{-1}\left(c\dot{x} + kx + f_p\right) + h + \left(T_{em}^{-1} - \widehat{T}_{em}^{-1}\right)m\ddot{x}$$

Note that H includes dynamic parameters, the hysteresis nonlinear effect of PEA, and the other unmodeled disturbances. They can all be regarded as lumped disturbances. $\dot{H}$is bounded and $\left|\dot{H}\right| \le \psi$. We can clearly observe that it is difficult to obtain an accurate model. Therefore, we try to propose a new control scheme without a system dynamics model to realize the accurate trajectory tracking of PDA.

2.2. TDE Framework

Aiming at the above difficulties, we propose a control framework without a system dynamic model using TDE. Specifically, the mathematical expression is as follows:

$$\widehat{H} \cong H_{(t-\Delta t)} \tag{4}$$

where Δt is delayed time. The lumped disturbances are directly estimated by $H_{(t-\Delta t)}$.

In engineering, the scheme can be efficient when Δt is selected very small [39]. We denote $\widehat{T}_{em}^{-1}m$ as $\overline{M}$. Substituting Eq. (4) into Eq. (3), we can obtain:

$$\widehat{H} = u_{(t-\Delta t)} - \overline{M}\ddot{x}_{(t-\Delta t)} \tag{5}$$

where $u_{(t-\Delta t)}$ is easily obtained by the delay value of u. But $\ddot{x}_{(t-\Delta t)}$ can't be obtained by actual observation. Therefore, numerical differentiation is usually used as follows [38]:

$$\ddot{x}_{(t-\Delta t)} = \begin{cases} \dfrac{x_t - 2x_{(t-\Delta t)} + x_{(t-2\Delta t)}}{\Delta t^2} t > 2\Delta t \\ 0 t \le 2\Delta t \end{cases} \tag{6}$$

The approximate errors of Eq. (6) are directly proportional to $O(\Delta t^2)$. In engineering, Δt usually selects a small value. Therefore, the errors can be ignored. Numerical differentiation will amplify noise, which can be settled by setting a smaller$\overline{M}$and adding a low-pass filter.

2.3. Proposed AFSTA-FONTSM scheme

To obtain more superior dynamic characteristic, we apply the FONTSM manifold as follows [38]:

$$s = \dot{e} + \alpha_1 D^{\lambda_1}[sig(e)^{\sigma_1}] + \alpha_2 D^{\lambda_2 - 1}[sig(e)^{\sigma_2}] \tag{7}$$

where $\alpha_1,\alpha_2,\lambda_1,\lambda_2,\sigma_1,\sigma_2$ are positive parameters, and satisfy the following condition: $0 < \lambda_1, \lambda_2, \sigma_1, \sigma_2 < 1$.$e = x_d - x \in \mathbf{R}$, x_d is desired trajectory, and$x$is actual trajectory. $sig(x)^y = |x|^y \mathrm{sign}(x) \in \mathbf{R}$, $D^x(y)$represent fractional-order operator.

The above FONTSM manifold has been verified to effectively ensure higher control accuracy and faster convergence speed. To suppress control chattering and achieve fixed-time convergence in the sliding mode phase, FSTA is used as the reaching law to ensure control timeliness [33,34]:

$$\begin{aligned} \dot{s} &= -k_1|s|^{1/2}\mathrm{sign}(s) - k_2|s|^p\mathrm{sign}(s) + \omega, s(t_0) = s_0 \\ \dot{\omega} &= -\frac{k_3}{2}\mathrm{sign}(s) + \varphi,\ \omega(t_0) = \omega_0 \end{aligned} \tag{8}$$

where$k_1, k_2, k_3 > 0$and$p > 1$. φsatisfy Lipschitz disturbances.

To estimate the convergence time of FSTA, we will make the following definitions:

Definition 2.1. $\forall s_0 \in \mathbf{R}, \exists T(s_0)$, such that $(s(t) \in \mathbf{R}) = 0$, and it is also satisfied for all $t \ge T$, at which the STA is regarded as finite-time convergence to the origin.

Definition 2.2. $\forall s_0 \in \mathbf{R}$, $\exists T$(explicitly indicated), such that $(s(t) \in \mathbf{R}) = 0$, and it is also satisfied for all $t \ge T$, at which the STA is regarded as fixed-time convergence to the origin.

Definition 2.3. $\forall s_0 \in \mathbf{R}$, $\exists T$(explicitly indicated), such that $(s(t) \in \mathbf{R}) \in (S \subset \mathbf{R})$, and it is also satisfied for all $t \ge T$, at which the STA is regarded as fixed-time convergence to the neighborhood$S$of the origin.

If the disturbance is bounded, Eq. (8) converges to the neighborhood of the origin in fixed-time.

Proof. The upper bound estimation of convergence time is given in the Appendix B.

As mentioned in [39], constant gains k_1 and k_3 are used. However, it is necessary to know the upper bound value of lumped disturbances when determining k_1 and k_3. Due to the upper bound value of lumped disturbances being difficult to obtain in engineering, the constant value may overestimate the control gains, thus increasing the chattering of the system.

To settle this problem, we proposed a new adaptive algorithm. When the control performance becomes worse, the gains should be increased to obtain higher convergence accuracy and faster response. On the contrary, it should be decreased rapidly to ensure stable performance and suppress noise effects. Specifically, the adaptive algorithm is as follows:

$$\dot{\widehat{k}}_1 = \begin{cases} \frac{\eta_1}{\sqrt{2}}\text{sign}(|s|-\mu) \text{if} \widehat{k}_1 > k_m \text{or} |s| > \mu \\ 0 \text{if} \widehat{k}_1 \le k_m \text{and} |s| \le \mu \end{cases} \tag{9}$$

$$\widehat{k}_3 = 2\varepsilon\widehat{k}_1 + 2\varepsilon k_2 \varepsilon_1^{(p-1/2)} \tag{10}$$

where ε,ε_1,η_1,$\mu$are arbitrary positive parameters. $k_m$is the lower bound of$\widehat{k}_1$.

In addition, if $|s_0| > \mu$, $\widehat{k}_1$needs to satisfy the following conditions:

$$\widehat{k}_1 > \frac{-\lambda k_2 \varepsilon_1^{p-1/2} - (4L+1)\varepsilon}{\lambda(1-\delta)} + \frac{(-\lambda - 4\varepsilon^2 - 2L)^2}{8\varepsilon\lambda(1-\delta)} \tag{11}$$

whereδ, λ, ε are arbitrary positive constants, and $0 < \delta < 1$.

The upper bound estimation of convergence time can be given by the following Theorem.

Theorem 2.1. Consider Eq. (8) exist a disturbance upper bound L, $\forall s_0 \in \mathbf{R}$, $\exists \mu \ge 0$, such that $s(t)$ converge to the neighborhood of the origin in fixed-time.

$$T_f \le \frac{1}{k_2(p-1)\varepsilon_1^{p-1}} + \frac{2}{\beta}\left[(\lambda + 4\varepsilon^2)\varepsilon_1 + \frac{M^2}{k_2^2(p-1)^2\varepsilon_1^{2(p-1)}} - 4\varepsilon\varepsilon_1^{1/2}\frac{M}{k_2(p-1)\varepsilon_1^{p-1}}\right]^{1/2} \tag{12}$$

where $\varepsilon_1 \ge \mu$.

$$M = \varepsilon\left(\frac{\eta_1}{\sqrt{2}}, \frac{1}{k_2(p-1)\varepsilon_1^{p-1}}\right) + \varepsilon k_2 \varepsilon_1^{p-1/2} + L$$

Proof. The detailed proof of Theorem 2.1 is given in the Appendix B.

Remark 2.1. Note that the applicable condition of Theorem 2.1 is that Eq. (11) is satisfied when $t_0 \ge 0$. If Eq. (11) is not satisfied at $t = 0$, the adaptive gain $\widehat{k}_1$ will be increased based on Eq. (9) until Eq. (11) is satisfied at t_0. t_0 can be estimated as:

$$t_0 \le \frac{\sqrt{2}}{\eta_1}\left[\frac{-\lambda k_2 \varepsilon_1^{p-1/2} - (4L+1)\varepsilon}{\lambda(1-\delta)} + \frac{(-\lambda - 4\varepsilon^2 - 2L)^2}{8\varepsilon\lambda(1-\delta)} - \widehat{k}_1(0)\right] \tag{13}$$

Because L exists, t_0 can be estimated. Otherwise, Eq. (11) will be satisfied in some finite-time, which exists but is unknown.

Combining Eq. (3), Eq. (5), Eqs. (7–10), a new AFSTA-FONTSM control scheme is proposed as follows:

$$u = \overline{M}\ddot{x} + \widehat{H} \tag{14}$$

Therefore, the final control law can be expressed as follows:

$$\begin{aligned} u = \overline{M}\big(&\ddot{x}_d + \alpha_1 D^{\lambda_1+1}[sig(e)^{\sigma_1}] + \alpha_2 D^{\lambda_2}[sig(e)^{\sigma_2}] \\ &+ \widehat{k}_1|s|^{1/2}\text{sign}(s) + k_2|s|^p\text{sign}(s) + \frac{\widehat{k}_3}{2}\int \text{sign}(s)\Big) \\ &+ u_{(t-\Delta t)} - \overline{M}\ddot{x}_{(t-\Delta t)} \end{aligned} \tag{15}$$

The block diagram of the time-delay control scheme based on AFSTA-FONTSM is shown in Fig. 2.

Remark 2.2. To obtain the relatively satisfactory control parameters of the proposed control scheme, the following adjustment processes are adopted:

Step (1): Let $\sigma_1 = \sigma_2 = \alpha_1 = \alpha_2 = 1$, $\widehat{k}_1 = k_2 = \widehat{k}_3 = 0$. λ_1 andλ_2 applies the data from [38,40]. $\overline{M}$starts from a small value and increases in turn until the control performance deteriorates. An adjustment process similar to$\overline{M}$can be used to determine$\alpha_1$andα_2;.

Step (2): Keep $\widehat{k}_1 = k_2 = \widehat{k}_3 = 0$, σ_1,$\sigma_2$decrease from 1 in turn, and observe the control performance;.

Step (3): Keep $k_2 = \widehat{k}_3 = 0$, set an appropriate k_m according to the control performance. η_1 increases from 0 in turn and μ decreases from a large value to a small value, while observing the control performance. k_2 is effectively determined by the same adjustment process asη_1.

Step (4): ε increases from 0 in turn until the control performance is observed to deteriorate. ε_1 and p can be determined by the same adjustment process asε.

Through the above processes, the control parameters can be adjusted. If the control performance does not meet the standards, the above processes should be repeated.

2.4. Discussion of proposed control scheme

(1) Discussion with the existing MSTA-FONTSM control scheme.

The proposed AFSTA-FONTSM is compared with the recently proposed control scheme from [38], namely MSTA-FONTSM. The control law of MSTA-FONTSM is rewritten as follows:

$$\begin{aligned} u = \overline{M}\big(&\ddot{x}_d + \alpha_1 D^{\lambda_1+1}[sig(e)^{\sigma_1}] + \alpha_2 D^{\lambda_2}[sig(e)^{\sigma_2}] \\ &+ k_1|s|^{1/2}\text{sign}(s) + k_2 s + k_3\int \text{sign}(s)dt + k_4\int sdt\Big) \\ &+ u_{(t-\Delta t)} - \overline{M}\ddot{x}_{(t-\Delta t)} \end{aligned} \tag{16}$$

Compared with MSTA-FONTSM, the proposed AFSTA-FONTSM has the following two advantages:

2.5. Control timeliness

Both control schemes adopt FONTSM error dynamics and have been proven to have faster response speed and higher accuracy than linear error dynamics. However, MSTA is finite-time convergence, and the convergence time is related to the initial value. Therefore, for a large initial value, the convergence time may also become longer and the control timeliness will become worse. The proposed AFSTA-FONTSM can ideally ensure control timeliness.

2.6. Flexibility of parameters

MSTA-FONTSM needs to obtain the upper bound value of lumped disturbances to determine the control gains. This work can be extremely difficult. The constant control parameters may overestimate the control gains, thus leading to chattering and affecting control accuracy. Compared with MSTA-FONTSM, the proposed AFSTA-FONTSM enjoys good parameter flexibility and no longer needs the upper bound value of lumped disturbances.

(2) Discussion with the existing AMSTA/ASTA-FONTSM control schemes.

The proposed AFSTA-FONTSM is compared with the recently pro-

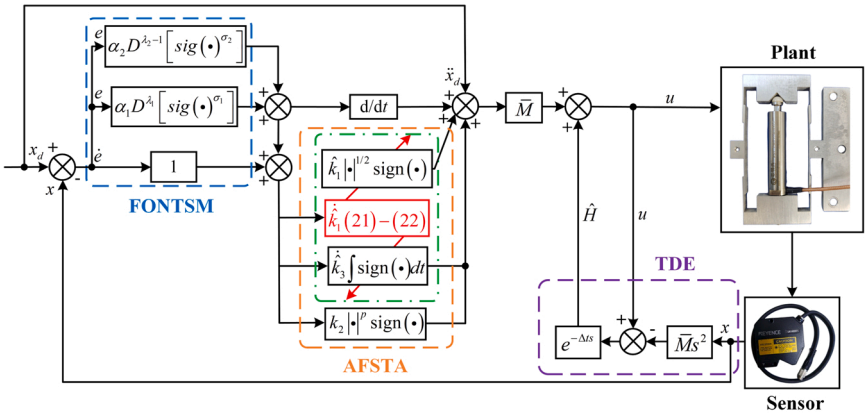

Fig. 2. Control scheme block diagram.

posed adaptive control scheme from [40,41] , referred to as AMSTA-FONTSM and ASTA-FONTSM respectively. The control law of AMSTA-FONTSM can be given as [40]:

$$u = \overline{M}\left(\ddot{x}_d + \alpha_1 D^{\lambda_1+1}[sig(e)^{\sigma_1}] + \alpha_2 D^{\lambda_2}[sig(e)^{\sigma_2}] + k_1|s|^{1/2}\text{sign}(s) + k_2 s + \widehat{\rho}(s)\text{sign}(s)\right) + u_{(t-\Delta t)} - \overline{M}\ddot{x}_{(t-\Delta t)} \tag{17}$$

The adaptive gain $\widehat{\rho}$ can be express as [40]:

$$\dot{\widehat{\rho}} = \vartheta|s| - \vartheta\phi\upsilon\widehat{\rho}, \widehat{\rho} = \rho_{\max}\text{sat}(\widehat{\rho}/\rho_{\max}) \tag{18}$$

where ϑ, ϕ, υ are positive parameters, and$\rho_{\max}$is the upper bound value of the adaptive gain$\widehat{\rho}$; sat(□)is the saturation function.

The control law of ASTA-FONTSM can be given as [41]:

$$u = \overline{M}\left(\ddot{x}_d + \alpha_1 D^{\lambda_1+1}[sig(e)^{\sigma_1}] + \alpha_2 D^{\lambda_2}[sig(e)^{\sigma_2}] + \widehat{k}_1|s|^{1/2}\text{sign}(s) + \widehat{k}_2\text{sign}(s)\right) + u_{(t-\Delta t)} - \overline{M}\ddot{x}_{(t-\Delta t)} \tag{19}$$

The adaptive gain $\widehat{k}_1$ and $\widehat{k}_2$ can be express as [41]:

$$\dot{\widehat{k}}_1 = \begin{cases} -\theta_1, \text{if}\widehat{k}_1 \geq k_{1\,\max} \\ -\theta_2, \text{if}k_{1\,\min} < \widehat{k}_1 < k_{1\,\max}, |s| < \Delta \\ \theta_1, \text{if}\widehat{k}_1 \leq k_{1\,\min}\text{or}k_{1\,\min} < \widehat{k}_1 < k_{1\,\max}, |s| \geq \Delta \end{cases} \tag{20}$$

$$\widehat{k}_2 = \theta_3\widehat{k}_1 \tag{21}$$

where θ_1,θ_2,θ_3,$\Delta$are positive parameters; $\widehat{k}_{1\,\min}$and $\widehat{k}_{1\,\max}$represent the minimum and maximum values of $\widehat{k}_1$. θ_1 and $\theta_2$stand for different speed parameters.

The proposed AFSTA-FONTSM is compared with AMSTA/ASTA-FONTSM in the following two aspects:

1) **Control timeliness**
   AMSTA and ASTA have also been proven to be finite-time convergence from [40] and [41] respectively. As previously analyzed, the control timeliness of the two algorithms is worse than the proposed AFSTA.
2) **Adaptive algorithm**

The saturation function is used in the adaptive algorithm of AMSTA, which may cause chattering and even destroy the hardware system. To suppress chattering, bound layer technology is selected, which will lead to the loss of stability in finite-time convergence and a decrease in control performance [42]. In addition, the adaptive algorithm of AMSTA is a low-pass-filter-like structure. Hence, it can't reflect the control system accurately and in real-time, which may lead to overestimation of the control gains and deterioration of the control performance. On the contrary, the adaptive algorithm of AFSTA has a principle similar to Eq. (20). The advantage can not only ensure timeliness but also reflect the control performance accurately and in real-time without overestimating the gains.

The above discussions will be verified by the following simulations and experiments.

3. Simulation demonstration

3.1. Simulation setup

We compare the two kinds of MSTA and STA used in [38], [40] and [41] with FSTA. The specific forms are summarized in the following Table 1.

We designed the following two simulation scenes. Scene one: the simulation is run with a small initial value $s_0 = 10$,$\omega_0 = 0$and disturbance $\xi = 3\sin(t)$, so that $L = 3$. Scene two: the disturbance is unchanged, and the large initial value $s_0 = 200$ and $\omega_0 = 0$ are performed to further analyze the influence of the initial value on the convergence results. The sampling time of the system simulation is set to 0.1 ms. The gains of FSTA are selected as $k_1 = 10$, $k_2 = 10$,$k_3 = 10$, $p = 1.5$. For the sake of fairness, the four algorithms should ensure that the gains of the corresponding positions are consistent. Specially, $k_4 = 1$.

3.2. Result and discussion

The simulation time of scene one is set to 2 s, and the simulation results are shown in Fig. 3.

As depicted in Fig. 3, the sliding mode variable s of four algorithms can converge to the neighborhood of the origin. Under the disturbance, the slight fluctuation of intermediate variable ω will not affect the convergence accuracy of s. The convergence time of the four algorithms is $T_{STA} = 0.7006$s, $T_{MSTA1} = 0.2961$s, $T_{MSTA2} = 0.3603$s, and $T_{FSTA} = 0.2549$s, respectively. FSTA can provide the fastest convergence speed under the same gains.

Table 1
Specific Forms of Algorithm.

Reference	Name	Algorithm Form
[41]	STA	$\dot{s} = -k_1\lvert s\rvert^{1/2}\text{sign}(s) + \omega$ $\dot{\omega} = -k_2\text{sign}(s) + \varphi$
[40]	MSTA1	$\dot{s} = -k_1\lvert s\rvert^{1/2}\text{sign}(s) - k_2 s + \omega$ $\dot{\omega} = -k_3\text{sign}(s) + \varphi$
[38]	MSTA2	$\dot{s} = -k_1\lvert s\rvert^{1/2}\text{sign}(s) - k_2 s + \omega$ $\dot{\omega} = -k_3\text{sign}(s) - k_4 s + \varphi$
[33,34]	FSTA	$\dot{s} = -k_1\lvert s\rvert^{1/2}\text{sign}(s) - k_2\lvert s\rvert^{p}\text{sign}(s) + \omega$ $\dot{\omega} = -\frac{k_3}{2}\text{sign}(s) + \varphi$

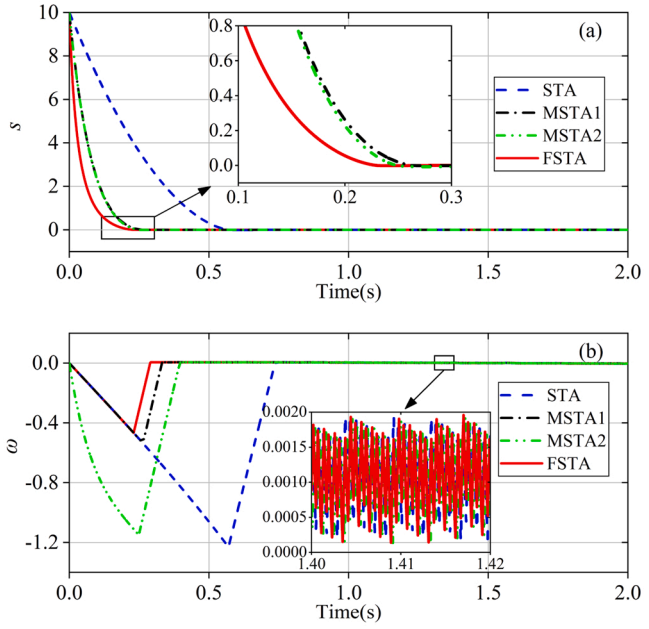

Fig. 3. Simulation results of scene one. (a) Sliding mode variable s; (b) Intermediate variable ω.

The simulation time of scene two is set to 10 s, and the simulation results are shown in Fig. 4.

Fig. 4 shows that the sliding mode variable s of the four algorithms can still converge to the neighborhood of the origin, completely. The convergence time is $T_{STA} = 5.3217$s,$T_{MSTA1} = 0.5068$s,$T_{MSTA2} = 4.5556$s and $T_{FSTA} = 0.3108$s, respectively. The increase percentage of convergence time is $P_{STA} = 659.59\%$, $P_{MSTA1} = 71.16\%$,$P_{MSTA2} = 1164.39\%$ and $P_{FSTA} = 21.93\%$, respectively. STA, MSTA1, and MSTA2 belong to finite-time convergence. MSTA1 and MSTA2 add closed-loop feedback terms, which effectively improve the convergence speed. However, the convergence time whose upper estimate is still related to the initial value. Therefore, the three algorithms are greatly influenced by the initial value. For a large initial value, FSTA still has a strong advantage in convergence speed.

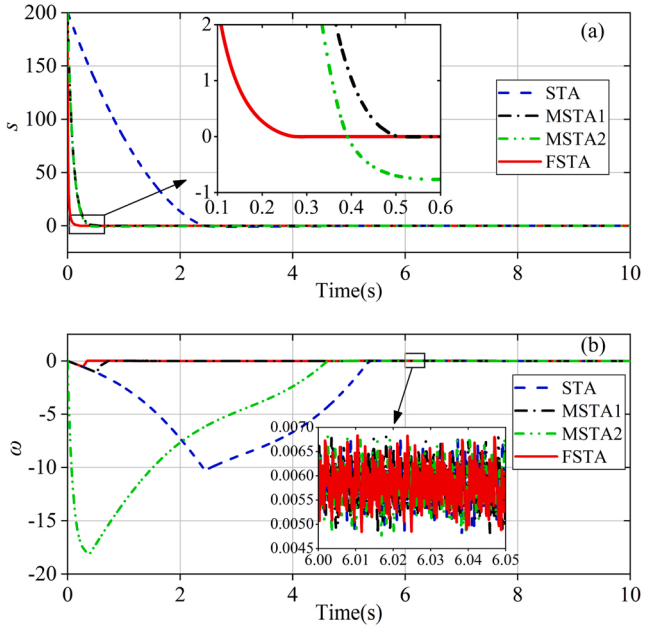

Fig. 4. Simulation results of scene two. (a) Sliding mode variable s; (b) Intermediate variable ω.

To conclude, the simulation results demonstrated that FSTA is superior to the existing super-twisting-like algorithms. When the disturbance is bounded, the upper bound estimation of the convergence time of FSTA is independent of the initial value. It has a faster convergence speed and can ensure control timeliness.

4. Experimental demonstration

4.1. Experimental setup

The experiments take a PDA as plant (see Fig. 5).

The experimental system is briefly described as follows. The control signal of PEA is provided by a voltage amplifier. The displacement is measured by a laser sensor in real-time. The signal needs to be preprocessed by the signal conditioner and collected by the analog-to-digital converter channel of the data acquisition card. A digital-to-analog converter channel outputs a control signal, which is passed through a voltage amplifier. The control program is developed in MATLAB/Simulink of the host personal computer and downloaded to the target computer by TCP/IP after the program is compiled. The sampling frequency of the system is set to 10 kHz. The experimental instruments are depicted in Fig. 6.

We perform experiments to compare the above four control schemes. The parameters of FONTSM and$\overline{M}$are selected as follows: $\lambda_1 = 0.01$,$\lambda_2 = 0.99$,$\sigma_1 = \sigma_2 = 0.95$,$\alpha_1 = \alpha_2 = 1$, $\overline{M} = 0.004$. The delayed time Δt is set to 0.1 ms. The parameters of the proposed AFSTA-FONTSM (see Eqs. (9, 10, 15)) are as follows: $k_m = 190$, $k_2 = 0.1$,$p = 1.5$,$\mu = 0.00025$,$\varepsilon_1 = 0.1$,$\varepsilon = 0.006$,$\eta_1 = 30$. To ensure fairness, the setting of other parameters should be the same as the proposed AFSTA-FONTSM. To be specific, the parameters of MSTA-FONTSM (see Eq. (16)) are selected as follows: $k_1 = 190$,$k_2 = 0.1$,$k_3 = 0.15$,$k_4 = 5$; The parameters of AMSTA-FONTSM (see Eq. (17-18)) are selected as follows: $k_1 = 190$,$k_2 = 0.1$,$\vartheta = 100$, $\phi = 0.1$,$\upsilon = 20$,$\rho_{\max} = 200$; The parameters of ASTA-FONTSM (see Eqs. (19–21)) are selected as follows: $k_{1\ \min} = 190$, $k_{1\ \max} = 220$,$\Delta = 0.00025$,$\theta_1 = 25$,$\theta_2 = 50$,$\theta_3 = 0.012$.

To demonstrate the reliability and superiority of the proposed AFSTA-FONTSM, four experimental scenes are designed as follows. Scene one: We use the above four schemes to control PDA to track a step trajectory and to evaluate the dynamic response of the system. Scene two: The above four schemes are also used to control PDA to track a slow cosine trajectory with a period of T = 2 s without load. Then, the tracking abilities of the four control schemes for a continuous trajectory are compared and analyzed. Scene three: A relatively fast cosine trajectory (T = 1 s) is tracked to further compare the control performance of the four schemes. Scene four: The constant load and monotonically increasing load are exerted on PDA respectively to confirm the robustness of the proposed AFSTA-FONTSM to lumped disturbances. The robustness of the proposed AFSTA-FONTSM can be verified by comparing the control performance with load and without load.

4.2. Result and discussion

(1) *Analysis results of scene one*: We control PDA to track a step trajectory with an amplitude of 100 μm. The experimental results of scene one are shown in Fig. 7.

As depicted in Fig. 7, the four control schemes can realize step trajectory tracking. It can be intuitively observed that the best tracking performance can be obtained by using the proposed AFSTA-FONTSM because the tracking errors are always smaller than other control schemes. To quantitatively evaluate the dynamic response of the system, the rise time (Tr) and root-mean-square error (RMSE)= $\sqrt{\sum_{i=1}^{N} e_i^2/N}$ within a 1% errors range are taken as performance indicators. The analysis results are listed in Table 2.

From Table 2, the proposed AFSTA-FONTSM has the fastest rise time

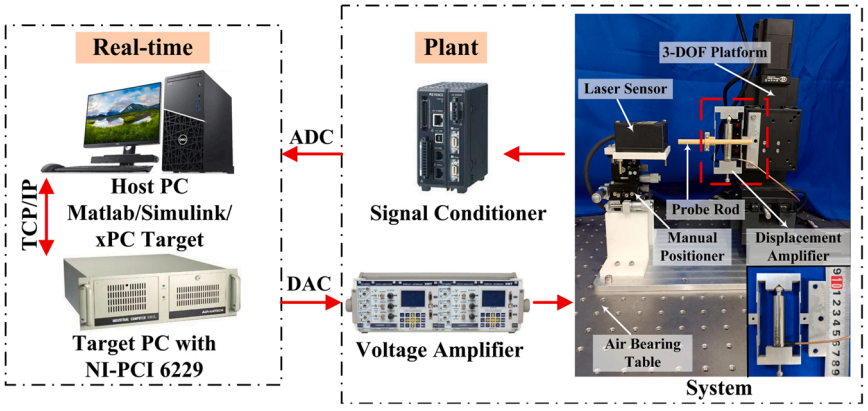

Fig. 5. Experimental system.

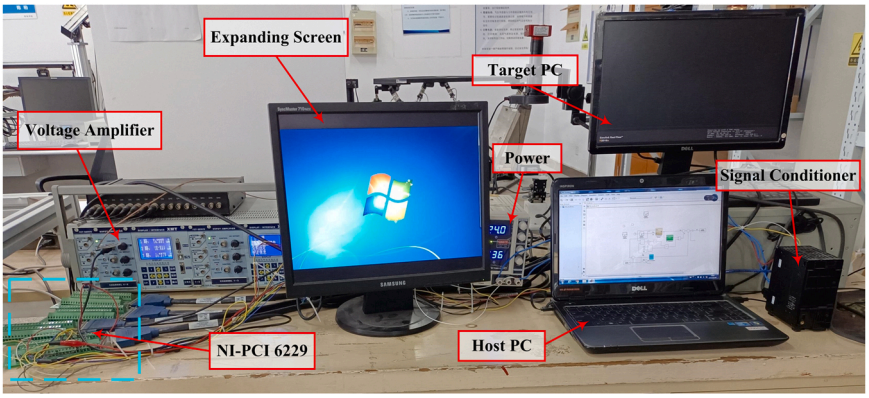

Fig. 6. Experimental instruments.

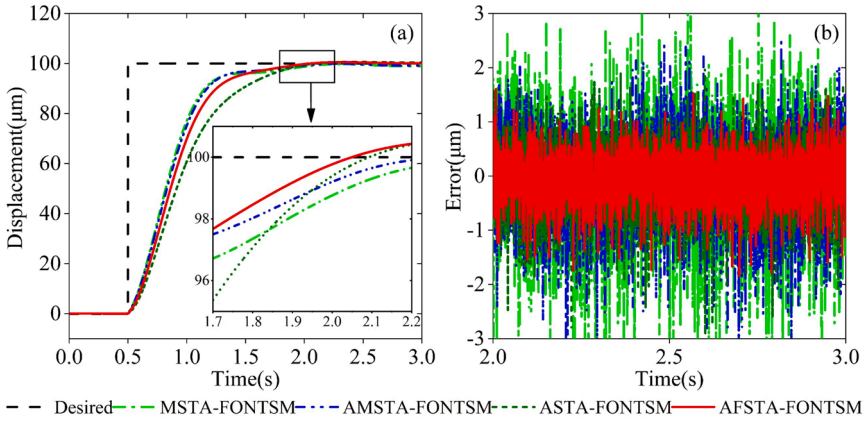

Fig. 7. Experimental results of scene one. (a) Trajectory tracking; (b) Tracking errors.

Table 2
Analysis results of performance indicators of step trajectory.

Signal	Indicator	Control Scheme			
		MSTA-FONTSM	AMSTA-FONTSM	ASTA-FONTSM	AFSTA-FONTSM
Step	Tr(s)	2.0399	1.9628	1.9558	1.8736
	RMSE (μm)	0.7529	0.5734	0.4435	0.3248

and the smallest RMSE, which is 1.8736 s and 0.3248 μm. The control performance of MSTA-FONTSM is the worst. Compared with MSTA-FONTSM, the rise time result of AMSTA-FONTSM, ASTA-FONTSM, and AFSTA-FONTSM is reduced by 3.78%, 4.12%, and 8.15%, respectively. For RMSE, the result of AMSTA-FONTSM, ASTA-FONTSM, and AFSTA-FONTSM is reduced by 23.84%, 41.09%, and 56.86%, respectively. The analysis results show that the proposed AFSTA-FONTSM has a better dynamic response than the other three control schemes.

(2) *Analysis results of scene two*: The desired trajectory is defined as $x_d = 50 - 50\cos(2\pi t)$. The experimental results of scene two are shown in Fig. 8.

As depicted in Fig. 8, the four control schemes have achieved

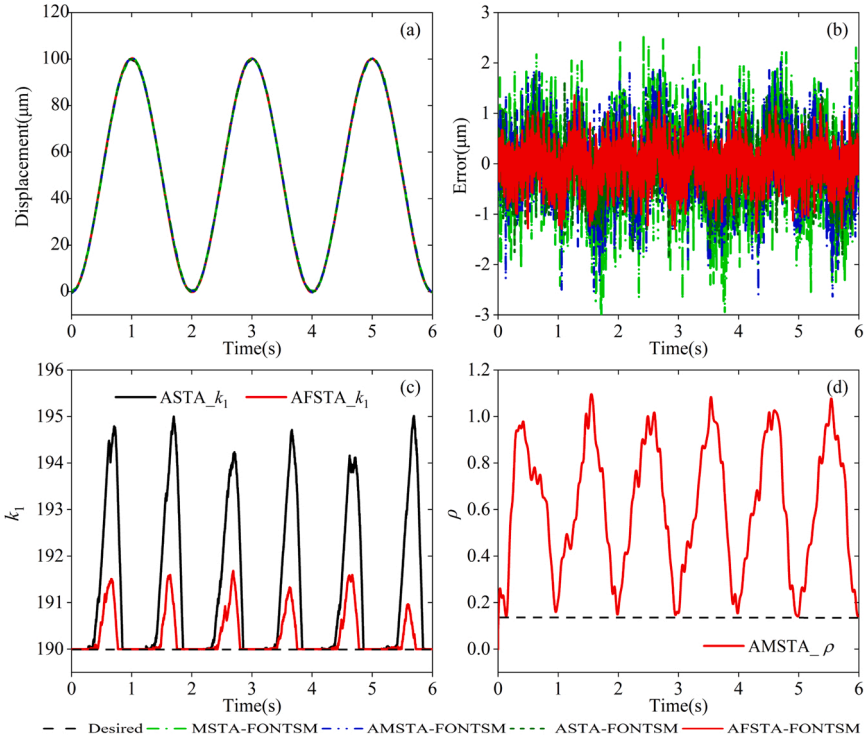

Fig. 8. Experimental results of scene two. (a) Trajectory tracking; (b) Tracking errors; (c) Adaptive gains of ASTA and AFSTA, $k_1 = \widehat{k}_1$; (d) Adaptive gain of AMSTA, $\rho = \widehat{\rho}$.

satisfactory control effects. The results verify that TDE technology, FONTSM error dynamics, and MSTA/AMSTA/ASTA/AFSTA control scheme can effectively realize the without a system dynamic model control of PDA with the hysteresis effect. It can be clearly that the proposed AFSTA-FONTSM has the smallest tracking errors among the four control schemes. For quantitative analysis, the following performance indicators are defined as: the RMSE, the absolute average error (AAE) $= \sum_{i=1}^{N}|e_i|/N$, the maximum error (MAX)$=$ MAX $\sum_{i=1}^{N}|e_i|$. The corresponding analysis results are given in Fig. 9.

In Fig. 9, control schemes 1, 2, 3, and 4 represent MSTA-FONTSM, AMSTA-FONTSM, ASTA-FONTSM, and AFSTA-FONTSM. The control performances of the three adaptive schemes are better than MSTA-FONTSM. Compared with MSTA-FONTSM, the RMSE result of

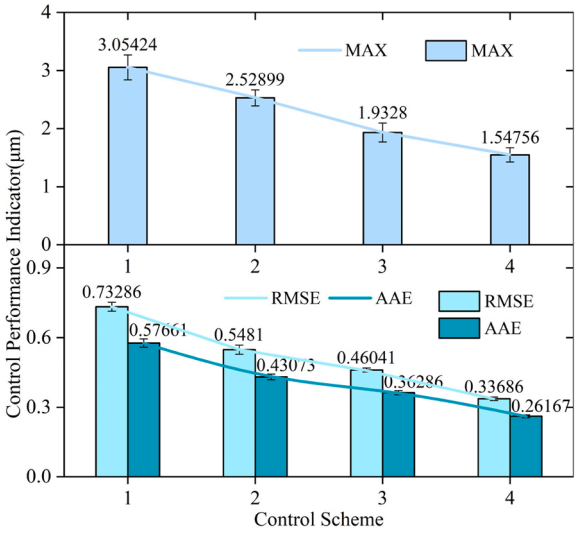

Fig. 9. Control performance of scene two.

AMSTA-FONTSM, ASTA-FONTSM, and AFSTA-FONTSM is reduced by 25.21%, 37.18%, and 54.03%, respectively. For AAE, the result of AMSTA-FONTSM, ASTA-FONTSM, and AFSTA-FONTSM is reduced by 25.30%, 37.07%, and 54.62%, respectively. The MAX result of AMSTA-FONTSM, ASTA-FONTSM, and AFSTA-FONTSM is reduced by 17.20%, 36.72%, and 49.33%, respectively.

It can be clarified that the proposed AFSTA-FONTSM can ensure high control accuracy and has the best control performance among the four control schemes. We further compare the adaptive algorithms as shown in Fig. 8(c) and (d). The proposed adaptive algorithm (see Eq. (9)) can update the control gains quickly and accurately according to real-time control performance. When the control performance tends to decrease, the adaptive gains are increased. On the contrary, they will quickly decrease to the lower bound value to guarantee a smooth control effect. Although the adaptive algorithm (see Eq. (20)) of ASTA-FONTSM can also realize the above updating process. Due to the performance of STA being worse than that of FSTA, the tracking errors are larger than that of AFSTA-FONTSM, which leads to larger control gains. In addition, the adaptive algorithm (see Eq. (18)) of AMSTA-FONTSM can also increase the control gains when the control performance deteriorates. However, there is still a non-zero gain of time-varying noise when the control performance is relatively perfect. This phenomenon is caused by the low-pass-filter structure, which may bring large noise control and performance deterioration even though the performance of MSTA is better than STA. Therefore, the proposed adaptive algorithm can obtain more satisfactory comprehensive performance compared with the existing ones. The above analysis results convincingly demonstrate the reliability and superiority of the proposed AFSTA-FONTSM, and this control scheme has high control accuracy.

(3) *Analysis results of scene three*: A relatively fast cosine trajectory (T = 1 s) is defined to further demonstrate trajectory tracking performance. The experimental results are shown in Fig. 10.

As shown in Fig. 10, the four control schemes can still have relatively satisfactory tracking effects. When the errors of the four control schemes slightly increase, the proposed AFSTA-FONTSM still has the smallest

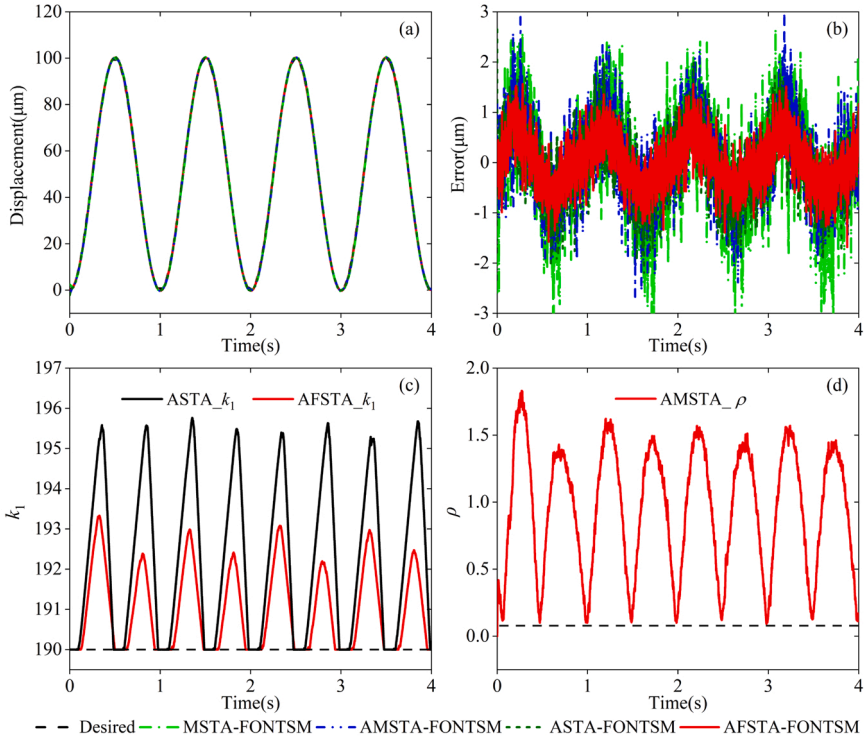

Fig. 10. Experimental results of scene three. (a) Trajectory tracking; (b) Tracking errors; (c) Adaptive gains of ASTA and AFSTA, $k_1 = \widehat{k}_1$; (d) Adaptive gain of AMSTA, $\rho = \widehat{\rho}$.

tracking errors. The above performance indicators continue to be used for analysis, and the corresponding results of scene three are shown in Fig. 11.

We can observe that the analysis results similar to that of Fig. 9 are given in Fig. 11. When tracking the relatively fast cosine trajectory, the control performance of the four control schemes decreases slightly. Therefore, the gains of the three adaptive algorithms are also increased compared with scene one. Nevertheless, the proposed adaptive algorithm can still ensure that AFSTA-FONTSM has the best comprehensive control performance. The results once again show that the proposed AFSTA-FONTSM has obvious advantages over the existing three control schemes.

(4) *Analysis results of scene four*: The mass of PDA is 0.096 kg. A load of 0.02 kg is exerted on the end of PDA. The desired trajectory is still a relatively fast ($T = 1$ s) cosine trajectory. Then, a low-density sponge with an initial weight of 0.0042 kg is added to the end of PDA while maintaining the desired trajectory unchanged. A peristaltic pump with 1.865 mL/s of constant flow is used to continuously inject water into the sponge. The control time is 4 s, which ensures the monotonically increasing disturbances from 0.042 kg to 0.012 kg. The experimental results of scene four are shown in Fig. 12. The corresponding control performance results are shown in Fig. 13.

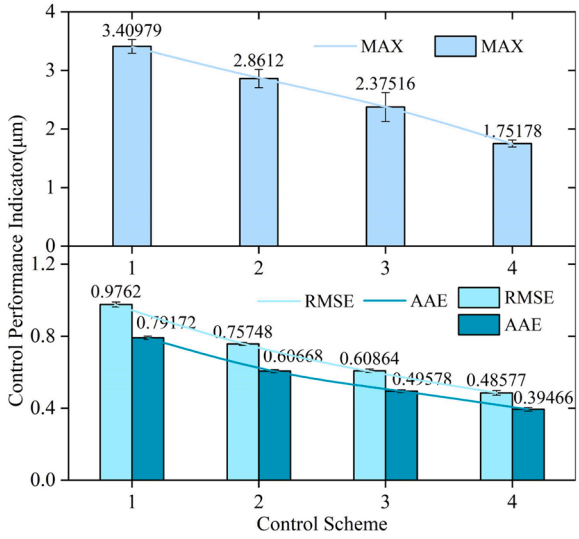

Fig. 11. Control performance of scene three.

As depicted in Fig. 12 and Fig. 13, the proposed AFSTA-FONTSM can still ensure satisfactory control performance under constant load and monotonically increasing load. The results strongly verify the robustness of the proposed AFSTA-FONTSM to lumped disturbances. Under the constant load, RMSE is increased by 10.94%, AAE is increased by 10.02%, and MAX is increased by 19.91% compared with scene three (without load). Under monotonically increasing load, RMSE is increased by 6.97%, AAE is increased by 4.74%, and MAX is increased by 10.25% compared with scene three.

In the case of load, the amplitude of RMSE and AAE is relatively small, while MAX increases relatively large, which is mainly affected by the proposed adaptive algorithm. When the tracking errors tend to decrease, the adaptive gains also decrease, which makes the amplitude of RMSE and AAE slightly increase. On the contrary, the adaptive gains speedily increase to suppress the tracking errors leading to the amplitude of MAX increases relatively large. The results demonstrate that the proposed adaptive algorithm can still effectively ensure control accuracy with lumped disturbances. In addition, the control performance of the proposed AFSTA-FONTSM under load is still better than the other three control schemes without load, which further shows the superiority of the proposed control scheme in robustness and control accuracy.

To conclude, the experimental results of the proposed AFSTA-FONTSM in the above four different scenes show satisfactory comprehensive control performance, which strongly demonstrates reliability and superiority compared with the existing three control schemes.

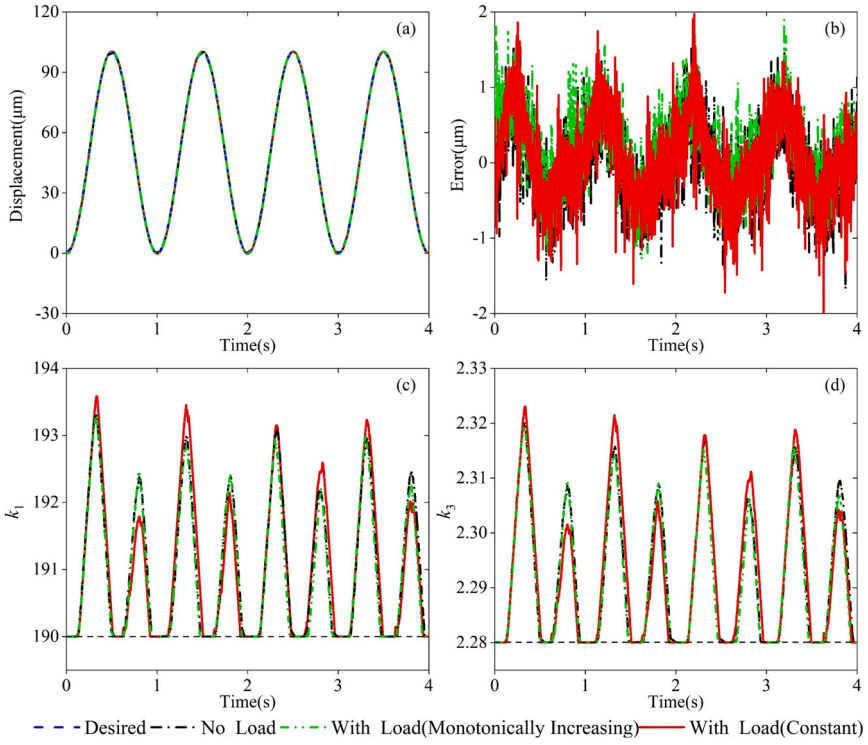

Fig. 12. Experimental results of scene four. (a) Trajectory tracking; (b) Tracking errors; (c) Adaptive gain of AFSTA, $k_1 = \widehat{k}_1$; (d) Adaptive gain of AFSTA, $k_3 = \widehat{k}_3$.

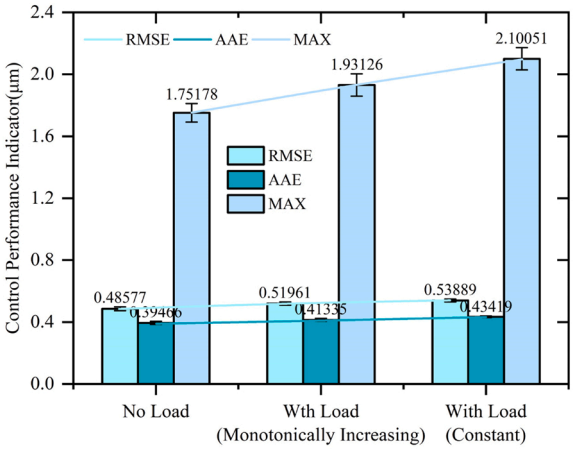

Fig. 13. Control performance of scene four.

5. Conclusion

To realize better control performance of PDA under complex lumped disturbances, this paper proposed a new time-delay control scheme using AFSTA and FONTSM. Firstly, TDE to estimate the lumped dynamic characteristic and a control framework without a system dynamic model is established. Next, the error dynamic characteristic with better performance is obtained by constructing the FONSTM manifold. Furthermore, a new AFSTA is proposed as the reaching law in the sliding mode phase. AFSTA has fixed-time convergence when the lumped disturbances are bounded, and the convergence time is independent of the initial value, which effectively ensures control timeliness. Meanwhile, the newly designed adaptive algorithm ensures that control gains no longer need the upper bound value of lumped disturbances, and will not lead to overestimation of control gains. Then, the convergence time of AFSTA is estimated and the stability of the closed-loop system is proved by the Lyapunov theory. Finally, we designed four scenes and performed comparative experiments with the recently proposed MSTA-FONTSM, AMSTA-FONTSM, and ASTA-FONTSM control schemes, verifying the reliability and superiority of the proposed AFSTA-FONTSM. For the step trajectory in scene one, the rise time and RMSE of the proposed AFSTA-FONTSM is 1.8736 s and 0.3248 μm respectively, which have better dynamic response than the other three control schemes. For the continuous cosine trajectory with a period of T = 2 s in scene two, RMSE, AAE, MAX are reduced by 54.03%, 54.62%, and 49.33% respectively compared with MSTA-FONTSM, which has the worst performance among the three control schemes. For the cosine trajectory (T = 1 s) in scene three, the control performance of the proposed AFSTA-FONTSM is still superior to the other three control schemes. For the constant load and monotonically increasing load in scene four, the proposed AFSTA-FONTSM can still ensure high control accuracy, even better than the other three control schemes without load. The experimental results show that the proposed AFSTA-FONTSM has the best comprehensive control performance and robustness.

It is worth noting that the TDE technique has an excellent effect on continuous nonlinear disturbances, such as gravity, Coriolis force, and so on. However, it is not perfect for discontinuous nonlinear disturbances, such as friction, mechanism clearance, and so on. This is also the limitation of the proposed work. But for PDA, the structure design adopts a flexible mechanism. Its advantage is that there is no friction and mechanism clearance, which fundamentally reduces other unmodeled disturbances. In future work, we will try to study the influence of discontinuous disturbances on TDE and compensate for TDE errors caused by discontinuous disturbances.

Declaration of Competing Interest

The author(s) declared no potential conflicts of interest with respect to the research, authorship, and/or publication of this article.

Acknowledgements

This work is supported by the National Natural Science Foundation of China (Grant No. 51975277, No. 52175097) and Natural Science Foundation of Jiangsu Province (Grant No. BK20210294).

Appendix A

Nomenclature	
piezoelectric displacement amplifier	PDA
piezoelectric actuator	PEA
sliding mode control	SMC
high-order SMC	HOSMC
super-twisting algorithm	STA
adaptive STA	ASTA
modified STA	MSTA
adaptive MSTA	AMSTA
fixed-time convergent STA	FSTA
adaptive fixed-time convergent super-twisting algorithm	AFSTA
fractional-order nonsingular terminal sliding mode	FONTSM
time-delay estimation	TDE
terminal sliding mode	TSM
nonsingular TSM	NTSM
rise time	Tr
root-mean-square error	RMSE
absolute average error	AAE
maximum error	MAX

Appendix B

Before stability analysis, the following Lemma is introduced.

Lemma [Lemma 2.1(a) of [43]]: The fractional integral operators I^a_{b+} and I^a_{c-} with $R(a) > 0$ are bounded in $L_q(b,c), 1 \le q \le \infty$:

$$\left\|I^a_{b+}y\right\|_q \le U\|y\|_q, \left\|I^a_{c-}y\right\|_q \le U\|y\|_q \left(U = \frac{(c-b)^{R(a)}}{R(a)|\Gamma(a)|}\right) \tag{22}$$

where $\Gamma(\cdot)$ is the Gamma function.

The proposed AFSTA-FONTSM control scheme (Eq. (15)) and adaptive algorithm (Eqs. (9, 10)) can be substituted into Eq. (8) to obtain:

$$\begin{aligned} \dot{s} &= -\widehat{k}_1|s|^{1/2}\mathrm{sign}(s) - k_2|s|^p\mathrm{sign}(s) + \omega \\ \dot{\omega} &= -\frac{\widehat{k}_3}{2}\mathrm{sign}(s) + \overline{\varphi} \end{aligned} \tag{23}$$

where $\overline{\varphi} = |d\xi(s,t)/dt| \le L(t-t_0), \xi = \overline{M}(H - \widehat{H})$ is the TDE errors.

Step 1: Consider $|s_0| > \varepsilon_1$, where $\varepsilon_1 > \mu, \mu > 0$ are constants. The Eq. (8) can be written as:

$$\begin{aligned} \frac{d|s(t)|}{dt} &= \frac{ds(t)}{dt}\mathrm{sign}(s(t)) \\ &= -k_1|s(t)|^{1/2} - k_2|s(t)|^p + \omega\mathrm{sign}(s(t)) \\ &\le -k_2|s(t)|^p \end{aligned} \tag{24}$$

For $t > t_0$, considering that the $\mathrm{sign}(s(t))$and $\mathrm{sign}(\omega(t))$ are opposite, that is $\omega(t)\mathrm{sign}(s(t)) < 0$. Eq. (24) can be solved as:

$$\frac{|s(t)|^{1-p}}{1-p} \le -k_2(t-t_0) + \frac{|s_0|^{1-p}}{1-p} \le -k_2(t-t_0) \tag{25}$$

then:

$$|s(t)|^{p-1} \le \frac{1}{k_2(p-1)(t-t_0)} \tag{26}$$

As $|s(t)|$ decrease to $|s(t)| = \varepsilon_1$ for a time $T_1 \le \frac{1}{k_2(p-1)\varepsilon_1^{p-1}}$, which is the first term of Eq. (12). It can observe that this term is independent of the initial value.

At the end of **Step 1**, $|s(t)| = \varepsilon_1 > 0$. When $t \in [t_0, T_1]$, the $\mathrm{sign}(s(t))$ and $\mathrm{sign}(\omega(t))$ are opposite. $|\omega(t)|$increases for $t \in [t_0, T_1]$ and satisfy $|\omega(T_1)| \le MT_1 \le M\frac{1}{k_2(p-1)\varepsilon_1^{p-1}}$, where M is the maximum speed of $\omega(t)$. Based on the Eqs. (8–10), M can be expressed as:

$$M = \frac{1}{2}\widehat{k}_3\left(\frac{1}{k_2(p-1)\varepsilon_1^{p-1}}\right) + L$$
$$= \frac{1}{2}\left[2\varepsilon\left(\frac{\eta_1}{\sqrt{2}}\frac{1}{k_2(p-1)\varepsilon_1^{p-1}}\right) + 2\varepsilon k_2\varepsilon_1^{p-1/2}\right] + L \tag{27}$$
$$= \varepsilon\left(\frac{\eta_1}{\sqrt{2}}\frac{1}{k_2(p-1)\varepsilon_1^{p-1}}\right) + \varepsilon k_2\varepsilon_1^{p-1/2} + L$$

If $\mu \le |s_0| \le \varepsilon_1$, **Step 1** is invalid. There will be no term $\frac{1}{k_2(p-1)\varepsilon_1^{p-1}}$in Eq. (12).

Step 2: To prove the stability of the system and facilitate the analysis of the Lyapunov theory, the following new vector is defined:

$$z(t) = [z_1(t), z_2(t)]^T = \left[\left|s(t)\right|^{1/2}\mathrm{sign}\left(s(t)\right), \omega(t)\right]^T \tag{28}$$

Obviously, $\mathrm{sign}(z_1(t)) = \mathrm{sign}(s(t))$, Eq. (8) is written as:

$$\dot{z}_1(t) = \frac{1}{2|z_1(t)|}\left(-\widehat{k}_1 z_1(t) - k_2|z_1(t)|^{2p}\mathrm{sign}(z_1(t)) + z_2(t)\right)$$
$$\dot{z}_2(t) = -\frac{\widehat{k}_3}{2|z_1(t)|}z_1(t) + \overline{\varphi} \tag{29}$$

Rewrite Eq. (29) into matrix form as follows:

$$\dot{z}(t) = -\frac{1}{2|z_1(t)|}A(z,t)z_1(t) \tag{30}$$

where:

$$A(z,t) = \begin{bmatrix} -\left(\widehat{k}_1 + k_2|z_1(t)|^{2p-1}\right) & 1 \\ -(\widehat{k}_3 - \psi) & 0 \end{bmatrix}$$

$$\overline{\varphi} = |d\xi(s,t)/dt| = \frac{1}{2|z_1(t)|}\psi(t)z_1(t), |\psi(t)| \le 2L$$

Note: If $z_1(t)$ and $z_2(t)$ converge to the neighborhood of the origin in fixed-time, $s(t)$ and $\omega(t)$ also have the same convergence properties.

Now consider defining the following Lyapunov function:

$$V(z, \widetilde{k}_1, \widetilde{k}_3) = V_0(z) + \frac{1}{2}\widetilde{k}_1 + \frac{1}{2}\widetilde{k}_3 \tag{31}$$

where $\widetilde{k}_1 = \widehat{k}_1 - k_1, \widetilde{k}_3 = \widehat{k}_3 - k_3$.

$V_0(z)$ is defined as follows:

$$V_0(z) = \left(\lambda + 4\varepsilon^2\right)z_1{}^2 + z_2{}^2 - 4\varepsilon z_1 z_2 = z^T P z \tag{32}$$

where:

$$P = \begin{bmatrix} \lambda + 4\varepsilon^2 & -2\varepsilon \\ -2\varepsilon & 1 \end{bmatrix}$$

The derivative of Eq. (32) can be expressed as:

$$\dot{V}_0(z) = \dot{z}^T P z + z^T P \dot{z} = \frac{1}{2|z_1(t)|}z^T\left[A^T(z)P + PA(z)\right]z$$
$$= -\frac{1}{2|z_1(t)|}z^T Q(z)z \tag{33}$$

$Q(z)$ is a symmetric matrix and expressed as:

$$Q(z) = A^T(z)P + PA(z) = \begin{bmatrix} Q_{11} & Q_{12} \\ Q_{12} & 4\varepsilon \end{bmatrix} \tag{34}$$

where:

$Q_{11} = 2\widehat{k}_1\lambda + 4\varepsilon(2\varepsilon\widehat{k}_1 - \widehat{k}_3) + 2(\lambda + 4\varepsilon^2)k_2|z_1(t)|^{2p-1} + 4\varepsilon\psi Q_{12} = \widehat{k}_3 - 2\varepsilon\widehat{k}_1 - 2\varepsilon k_2|z_1(t)|^{2p-1} - \lambda - 4\varepsilon^2 - \psi$

To ensure that the $Q(z)$ is positive definite, the adaptive gain $\widehat{k}_3$ is:

$$\widehat{k}_3 = 2\varepsilon\widehat{k}_1 + 2\varepsilon k_2\varepsilon_1^{p-1/2} \tag{35}$$

$Q(z)$ is the positive definite matrix, and the minimum eigenvalue satisfies $\mu_{\min}(Q) \ge 2\varepsilon$.

Using Rayleigh's inequality $z^T Q(z)z \ge \mu_{\min}(Q)\|z\|^2$, we can further obtain:

$$\dot{V}_0(z) = -\frac{1}{2|z_1(t)|}z^T Q(z)z \le -\frac{\varepsilon}{|z_1(t)|}\|z\|^2 \tag{36}$$

According to Rayleigh's inequality, $V_0(z) \le \mu_{\max}(p)\|z\|^2$ and $V_0^{1/2}(z) \le \sqrt{\mu_{\min}(p)}\|z\|$, $\dot{V}_0(z)$can be expressed as:

$$\dot{V}_0(z) \le -\beta V_0^{1/2}(z),$$

where

$$\beta = \varepsilon\frac{\sqrt{\mu_{\min}(P)}}{\mu_{\max}(P)} \tag{37}$$

Applying theory 12 proposed from [44], The convergence time of Eq. (37) is estimate as:

$$T_f(z(T_1)) \le \frac{2V_0^{1/2}(z(T_1))}{\beta} \tag{38}$$

According to the end of **Step 1**, $z_1(T_1)$ and $z_2(T_1)$ are bounded:

$$|z_1(T_1)| \le {\varepsilon_1}^{1/2}, |z_2(T_1)| \le M\frac{1}{k_2(p-1)\varepsilon_1^{p-1}} \tag{39}$$

so that:

$$V_0(z(T_1)) \le \left(\lambda + 4\varepsilon^2\right)\varepsilon_1 + \frac{M^2}{k_2^2(p-1)^2\varepsilon_1^{2(p-1)}} - 4\varepsilon\varepsilon_1^{1/2}\frac{M}{k_2(p-1)\varepsilon_1^{p-1}} \tag{40}$$

Therefore, the second term of Eq. (12) is obtained. The Eq. (8) converges to the neighborhood of origin, that is $|z_1| \le \mu^{1/2}$or $|s| \le \mu$ and $|z_2| \le \eta(\mu,L)$, where $\eta = \int_{t_0}^{T_f}(\widehat{k}_3(s)/2 + L)ds$; Theorem 2.1 is proved.

Note: The defined Lyapunov function is continuous but it does not satisfy the Lipschitz condition because Eq. (31) is differentiable everywhere besides $z = 0$. Therefore, Lyapunov's second method will be invalid. But, the convergent property can still be proved according to Zubov's theorem applied in [45], which only needs the Lyapunov function is continuous. In the meantime, the theories shown in [45] apply to the case that the derivative of the Lyapunov function does not exist. Please refer to [46] for more details.

The derivation of Eq. (41) is given:

$$\dot{V}(z,\widetilde{k}_1,\widetilde{k}_3) = \dot{V}_0(z) + \widetilde{k}_1\dot{\widehat{k}}_1 + \widetilde{k}_3\dot{\widehat{k}}_3 \tag{41}$$

and furthermore:

$$\dot{V}(z,\widetilde{k}_1,\widetilde{k}_3) \le -\beta V_0^{1/2}(z) - \frac{\eta_1}{\sqrt{2}}|\widetilde{k}_1| - \frac{\eta_2}{\sqrt{2}}|\widetilde{k}_3| + \widetilde{k}_1\dot{\widehat{k}}_1 + \widetilde{k}_3\dot{\widehat{k}}_3 + \frac{\eta_1}{\sqrt{2}}|\widetilde{k}_1| + \frac{\eta_2}{\sqrt{2}}|\widetilde{k}_3| \tag{42}$$

According to the following inequality:

$$\left(x^2+y^2+z^2\right)^{1/2} \le |x|+|y|+|z|$$

we can derive:

$$-\beta V_0^{1/2}(z) - \frac{\eta_1}{\sqrt{2}}|\widetilde{k}_1| - \frac{\eta_2}{\sqrt{2}}|\widetilde{k}_3| \le -\eta_0\sqrt{V(z,\widetilde{k}_1,\widetilde{k}_3)} \tag{43}$$

where $\eta_0 = \min(\beta,\eta_1,\eta_2)$. Therefore, Eq. (42) can be rewritten as:

$$\dot{V}(z,\widetilde{k}_1,\widetilde{k}_3) \le -\eta_0\sqrt{V(z,\widetilde{k}_1,\widetilde{k}_3)} + \widetilde{k}_1\dot{\widehat{k}}_1 + \widetilde{k}_3\dot{\widehat{k}}_3 + \frac{\eta_1}{\sqrt{2}}|\widetilde{k}_1| + \frac{\eta_2}{\sqrt{2}}|\widetilde{k}_3| \tag{44}$$

Since Eq. (8) is fixed-time convergence, the adaptive gains $\widehat{k}_1$ and $\widehat{k}_3$ are bounded. $\forall t \ge 0$, $\exists$ positive constants k_1,k_3, such that $\widehat{k}_1 - k_1 < 0$and $\widehat{k}_3 - k_3 < 0$. Based on the above analysis, Eq. (44) can be simplified as:

$$\dot{V}(z,\widetilde{k}_1,\widetilde{k}_3) \le -\eta_0\sqrt{(z,\widetilde{k}_1,\widetilde{k}_3)} + \zeta \tag{45}$$

where :

$$\zeta = -|\widetilde{k}_1|\left(\dot{\widehat{k}}_1 - \frac{\eta_1}{\sqrt{2}}\right) - |\widetilde{k}_3|\left(\dot{\widehat{k}}_3 - \frac{\eta_2}{\sqrt{2}}\right)$$

Case 1. Suppose that for $t \geq 0$, $|s| > \mu$. According to Eq. (9), we can be obtain:

$$\dot{\widehat{k}}_1 = \frac{\eta_1}{\sqrt{2}}, \zeta = -|\widetilde{k}_3|\left(\dot{\widehat{k}}_3 - \frac{\eta_2}{\sqrt{2}}\right) \tag{46}$$

$\varepsilon = \frac{\eta_2}{2\eta_1}$ is selected. The differential of Eq. (10) can be expressed as:

$$\dot{\widehat{k}}_3 = 2\varepsilon\dot{\widehat{k}}_1 = 2.\frac{\eta_2}{2\eta_1}.\frac{\eta_1}{\sqrt{2}} = \frac{\eta_2}{\sqrt{2}} \tag{47}$$

Therefore, $\zeta = 0$, Eq. (43) becomes:

$$\dot{V}(z, \widetilde{k}_1, \widetilde{k}_3) \leq -\eta_0\sqrt{(z, \widetilde{k}_1, \widetilde{k}_3)} \tag{48}$$

$\dot{V}(z, \widetilde{k}_1, \widetilde{k}_3)$ is negative definite and the system is asymptotically stable.

Case 2. Suppose that $|s| \leq \mu$, $\widehat{k}_1$ is calculated as follows:

$$\dot{\widehat{k}}_1 = \begin{cases} -\frac{\eta_1}{\sqrt{2}} \text{if} \widehat{k}_1 > k_m \text{or} |s| > \mu \\ 0 \text{if} \widehat{k}_1 \leq k_m \text{and} |s| \leq \mu \end{cases} \tag{49}$$

with:

$$\zeta = \begin{cases} 2|\widehat{k}_1 - k_1|\frac{\eta_1}{\sqrt{2}} \text{if} \widehat{k}_1 > k_m \text{or} |s| > \mu \\ |\widehat{k}_1 - k_1|\frac{\eta_1}{\sqrt{2}} \text{if} \widehat{k}_1 \leq k_m \text{and} |s| \leq \mu \end{cases} \tag{50}$$

In view of Eq. (45), the sign of Lyapunov function is indefinite. However, the validity of Eq. (50) only holds for a period of time. Because the adaptive gains $\widehat{k}_1$ and $\widehat{k}_3$ are decreased, $|s|$ will gradually become larger than μ. Once $|s|$ is larger than μ, Case 1 holds again. The system is still asymptotically stable, so on.

By combining $|s| \leq \mu$ with Eq. (7), we can obtain:

$$s = \dot{e} + \alpha_1 D^{\lambda_1}[sig(e)^{\sigma_1}] + \alpha_2 D^{\lambda_2 - 1}[sig(e)^{\sigma_2}], |s| \leq \mu \tag{51}$$

Eq. (51) can be rewritten in the following two forms:

$$\begin{aligned} &\dot{e} + \alpha_1 D^{\lambda_1}[sig(e)^{\sigma_1}] \\ &+\left(\alpha_2 - s\left(D^{\lambda_2 - 1}[sig(e)^{\sigma_2}]\right)^{-1}\right) D^{\lambda_2 - 1}[sig(e)^{\sigma_2}] = 0 \end{aligned} \tag{52}$$

$$\begin{aligned} &\dot{e} + \left(\alpha_1 - s\left(D^{\lambda_1}[sig(e)^{\sigma_1}]\right)^{-1}\right) D^{\lambda_1}[sig(e)^{\sigma_1}] \\ &+\alpha_2 D^{\lambda_2 - 1}[sig(e)^{\sigma_2}] = 0 \end{aligned} \tag{53}$$

If $\alpha_2 - s(D^{\lambda_2 - 1}[sig(e)^{\sigma_2}])^{-1} > 0$ holds, Eq. (52) is in the same form as Eq. (7). The system will converge to the FONTSM manifold (see Eq. (7)) until $\left|D^{\lambda_2 - 1}[sig(e)^{\sigma_2}]\right| \leq \alpha_2^{-1}\mu$. Select q of **Lemma** as $q = \infty$.

$$ess\sup\left|D^{\lambda_2 - 1}[sig(e)^{\sigma_2}]\right| \leq U ess\sup|e|^{\sigma_2} \tag{54}$$

where $ess\sup(\cdot)$ represents the essential maximum value.

Substituting $\left|D^{\lambda_2 - 1}[sig(e)^{\sigma_2}]\right| \leq ess\sup\left|D^{\lambda_2 - 1}[sig(e)^{\sigma_2}]\right|$ into Eq. (54):

$$\left|D^{\lambda_2 - 1}[sig(e)^{\sigma_2}]\right| \leq U ess\sup|e|^{\sigma_2} \tag{55}$$

A bounded time-varying variable $\varpi \geq 1$ is introduced to make Eq. (55) become an equality.

$$\left|D^{\lambda_2 - 1}[sig(e)^{\sigma_2}]\right| = \varpi^{-1} U ess\sup|e|^{\sigma_2} \tag{56}$$

Substituting $\left|D^{\lambda_2 - 1}[sig(e)^{\sigma_2}]\right| \leq \alpha_2^{-1}\mu$ into Eq. (56) can further obtain:

$$\varpi^{-1} U ess\sup|e|^{\sigma_2} \leq \alpha_2^{-1}\mu \tag{57}$$

Therefore, the error e will converge as follows:

$$|e| \leq |e|_{\max} \leq \left(\alpha_2^{-1}\mu\varpi U^{-1}\right)^{1/\sigma_2} \tag{58}$$

Similarly, we have $\left|D^{\lambda_1}[sig(e)^{\sigma_1}]\right| \leq \alpha_1^{-1}\mu$. Combining Eq. (7) and $\left|D^{\lambda_2 - 1}[sig(e)^{\sigma_2}]\right| \leq \alpha_2^{-1}\mu$, we can obtain:

$$|\dot{e}| \leq |s| + \left|\alpha_1 D^{\lambda_1}[\text{sign}(e)^{\sigma_1}]\right| + \left|\alpha_2 D^{\lambda_2 - 1}[\text{sign}(e)^{\sigma_2}]\right| = 3\mu \tag{59}$$

To sum up, the stability proof of the closed-loop system has been completed.

References

[1] Ling J, Feng Z, Chen L, Zhu Y, Pan Y. Neural network-based iterative learning control of a piezo-driven nanopositioning stage. Precis Eng 2023;81:112–23.
[2] Song Z, Li X, Yang X, Li Y, Wang L, Wu H. Kinematic modeling of a spatial three degrees-of-freedom compliant micro-motion parallel mechanism considering input coupling effect and bilateral restrained torsion. Ind Robot 2022;50(3):385–400.
[3] Andany SH, Nievergelt AP, Kangül M, Ziegler D, Fantner GE. A high-bandwidth voltage amplifier for driving piezoelectric actuators in high-speed atomic force microscopy. Rev Sci Instrum 2023;94(9):093703.
[4] Yang X, Wu H, Li Y, Kang S, Chen B, Lu H, et al. Dynamics and isotropic control of parallel mechanisms for vibration isolation. IEEE/ASME Trans Mechatron 2020;25 (4):2027–34.
[5] Yu S, Wu H, Xie M, Lin H, Ma J. Precise robust motion control of cell puncture mechanism driven by piezoelectric actuators with fractional-order nonsingular terminal sliding mode control. Bio-Des Manuf 2020;3(4):410–26.
[6] Wang G, Xu Q. Design and development of a piezo-driven microinjection system with force feedback. Adv Robot 2017;31(23-24):1349–59.
[7] Wang G, Xu Q. Design and precision position/force control of a piezo-driven microinjection system. IEEE/ASME Trans Mechatron 2017;22(4):1744–54.
[8] Xu Q. Micromachines for Biological Micromanipulation. Cham: Springer; 2018. p. 1.
[9] Kang S, Wu H, Yang X, Li Y, Wang Y. Model-free robust finite-time force tracking control for piezoelectric actuators using time-delay estimation with adaptive fuzzy compensator. Trans Inst Meas Control 2019;42(3):351–64.
[10] Ghafarirad H, Rezaei SM, Sarhan AADM, Mardi NA. Modified robust external force control with disturbance rejection with application to piezoelectric actuators. Trans Inst Meas Control 2014;37(1):131–43.
[11] Ling J, Feng Z, Zheng D, Yang J, Yu H, Xiao X. Robust adaptive motion tracking of piezoelectric actuated stages using online neural-network-based sliding mode control. Mech Syst Signal Proc 2021;150:107235.
[12] Naz S, Raja MAZ, Mehmood A, Zameer A, Shoaib M. Neuro-intelligent networks for Bouc–Wen hysteresis model for piezostage actuator. Eur Phys J 2021;136(4):1–20.
[13] Naz S, Raja MAZ, Mehmood A, Jaafery AZ. Intelligent predictive solution dynamics for dahl hysteresis model of piezoelectric actuator. Micromachines 2022;13(12): 2205.
[14] Feng Z, Liang W, Ling J, Xiao X, Tan KK, Lee TH. Integral terminal sliding-mode-based adaptive integral backstepping control for precision motion of a piezoelectric ultrasonic motor. Mech Syst Signal Proc 2020;144:106856.
[15] Flores G, Aldana N, Rakotondrabe M. Model predictive control based on the generalized Bouc-Wen model for piezoelectric actuators in robotic hand with only position measurements. IEEE Control Syst Lett 2022;6:2186–91.
[16] Wang J, Xiong C, Huang J, Peng J, Zhang J, Zhao P. Waveform design method for piezoelectric print-head based on iterative learning and equivalent circuit model. Micromachines 2023;14(4):768.
[17] Zhang L, Fei J. Intelligent complementary terminal sliding mode using multiloop neural network for active power filter. IEEE Trans Power Electron 2023;38(8): 9367–83.
[18] Guo R, Ding Y, Yue X. Active adaptive continuous nonsingular terminal sliding mode controller for hypersonic vehicle. Aerosp Sci Technol 2023;137:108279.
[19] Din SU, Khan Q, Rehman FU, Akmeliawanti R. A comparative experimental study of robust sliding mode control strategies for underactuated systems. IEEE Access 2017;6:1927–39.
[20] Wang Y, Yan F, Tian B, Gu L, Chen B. Nonsingular terminal sliding mode control of underwater remotely operated vehicles. Trans Can Soc Mech Eng 2018;42(2): 105–15.
[21] Deng W, Yao J, Ma D. Time-varying input delay compensation for nonlinear systems with additive disturbance: an output feedback approach. Int J Robust Nonlinear Control 2018;28(1):31–52.
[22] Edwards C, Shtessel YB. Adaptive continuous higher order sliding mode control. Automatica 2016;65:183–90.
[23] Edwards C, Shtessel Y. Enhanced continuous higher order sliding mode control with adaptation. J Frankl Inst-Eng Appl Math 2019;356(9):4773–84.
[24] Rinaldi G, Menon PP, Edwards C, Ferrara A, Shtessel Y. Adaptive dual-layer super-twisting sliding mode observers to reconstruct and mitigate disturbances and communication attacks in power networks. Automatica 2021;129:109656.
[25] Lu Y, Tan C, Ge W, Zhao Y, Wang G. Adaptive disturbance observer-based improved super-twisting sliding mode control for electromagnetic direct-drive pump. Smart Mater Struct 2022;32(1):017001.
[26] Adil HMM, Ahmed S, Ahmad I. Control of MagLev system using supertwisting and integral backstepping sliding mode algorithm. IEEE Access 2020;8:51352–62.
[27] Borlaug IG, Pettersen KY, Gravdahl JT. The generalized super-twisting algorithm with adaptive gains. Int J Robust Nonlinear Control 2022;32(13):7240–70.
[28] Liu D, Esche S, Wang M. An adaptive super-twisting algorithm based on conditioning technique. Trans Inst Meas Control 2021;44(2):497–505.
[29] Nagesh I, Edwards C. A multivariable super-twisting sliding mode approach. Automatica 2014;50(3):984–8.
[30] Wang Z, Yuan J, Pan Y. Adaptive second-order sliding mode control: a unified method. Trans Inst Meas Control 2017;40(6):1927–35.
[31] Yang Y, Qin S. A new modified super-twisting algorithm with double closed-loop feedback regulation. Trans Inst Meas Control 2016;39(11):1603–12.
[32] Cruz-Zavala E, Moreno JA, Fridman LM. Uniform robust exact differentiator. IEEE Trans Autom Control 2011;56(11):2727–33.
[33] Basin M, Bharath Panathula C, Shtessel Y. Multivariable continuous fixed-time second-order sliding mode control: design and convergence time estimation. IET Contr Theory Appl 2017;11(8):1104–11.
[34] Basin M, Rodriguez-Ramirez P, Garza-Alonso A. Continuous fixed-time convergent super-twisting algorithm in case of unknown state and disturbance initial conditions. Asian J Control 2019;21(1):323–38.
[35] Guerra-Avellaneda F, Basin M. Continuous fixed-time convergent control design for stochastic super-twisting system. J Frankl Inst-Eng Appl Math 2020;357(16): 11793–806.
[36] Jin M, Kang SH, Chang PH, Lee J. Robust control of robot manipulators using inclusive and enhanced time delay control. IEEE/ASME Trans Mechatron 2017;22 (5):2141–52.
[37] Ahmed S, Wang H, Tian Y. Model-free control using time delay estimation and fractional-order nonsingular fast terminal sliding mode for uncertain lower-limb exoskeleton. J Vib Control 2018;24(22):5273–90.
[38] Wang Y, Yan F, Zhu K, Chen B, Wu H. A new practical robust control of cable-driven manipulators using time-delay estimation. Int J Robust Nonlinear Control 2019;29(11):3405–25.
[39] Kali Y, Saad M, Benjelloun K, Khairallah C. Super-twisting algorithm with time delay estimation for uncertain robot manipulators. Nonlinear Dynam 2018;93(2): 557–69.
[40] Wang Y, Yan F, Jiang S, Chen B. Time delay control of cable-driven manipulators with adaptive fractional-order nonsingular terminal sliding mode. Adv Eng Softw 2018;121:13–25.
[41] Wang Y, Chen J, Yan F, Zhu K, Chen B. Adaptive super-twisting fractional-order nonsingular terminal sliding mode control of cable-driven manipulators. ISA Trans 2019;86:163–80.
[42] Yu S, Yu X, Shirinzadeh B, Man Z. Continuous finite-time control for robotic manipulators with terminal sliding mode. Automatica 2005;41(11):1957–64.
[43] Kilbas AA, Srivastava HM, Trujillo JJ. Fractional integrals and fractional derivatives. Theory and applications of fractional differential equations. 1st ed.,. Amsterdam, The Netherlands: Elsevier; 2006. p. 69–133.
[44] Polyakov A, Fridman L. Stability notions and Lyapunov functions for sliding mode control systems. J Frankl Inst-Eng Appl Math 2014;351(4):1831–65.
[45] Poznyak AS. Theorem 20.2. Advanced mathematical tools for automatic control engineers. Amsterdam, The Netherlands: Elsevier; 2008. p. 568.
[46] Moreno JA, Osorio M. Strict lyapunov functions for the super-twisting algorithm. IEEE Trans Autom Control 2012;57(4):1035–40.